CNRS
Centre National de la Recherche Scientifique

INFN
Istituto Nazionale di Fisica Nucleare

Conceptual design of the second stage of frequency stabilization for Advanced Virgo

VIR-0013C-12

Enrico Calloni[1], Gabriele Vajente[2]
[1] *Università di Napoli Federico II and INFN Napoli,* [2] *INFN Pisa*

Issue: C

Date: May 9, 2012

VIRGO * A joint CNRS-INFN Project
Via E. Amaldi, I-56021 S. Stefano a Macerata - Cascina (Pisa)
Secretariat: Telephone (39) 050 752 521 * FAX (39) 050 752 550 * Email W3@virgo.infn.it

Contents

1 Introduction **1**

2 Laser stabilization topology **1**
2.1 General description 1
2.2 Definition of terms 4
2.3 System equations 5

3 Requirements on laser frequency at ITF input **6**

4 Input ingredients **6**
4.1 Optical transfer functions 6
4.2 Actuation transfer functions 7

5 Control filters and stability **7**

6 Sensing and ADC-DAC noises **9**

7 Noise projections **13**

8 Conclusions and next steps **14**

1 Introduction

To cope with the very high stability requirement of the laser frequency with respect to the interferometer lengths [1], a second stage of frequency stabilization which uses an error signal coming from the interferometer itself is needed [2]. This notes describes the conceptual design of such a *second stage of frequency stabilization* (SSFS) system, following closely what was done for the Virgo system design [2].

2 Laser stabilization topology

2.1 General description

When the interferometer is locked and working in the final locking point (or even during the lock acquisition) the foreseen scheme for frequency stabilization consists in nesting three control loops with different band-widths and error signals. The use of such a technique is dictated by the need of maintaining the input mode cleaner on resonance for the laser frequency together with the interferometer.

When the injection system is running in stand-alone configuration the laser frequency is locked on the input mode cleaner (IMC) length by using a standard Pound-Drever-Hall (PDH) technique in reflection of the IMC cavity (pre-stabilization loop). In this way the laser frequency follows any length variation of the cavity. At low frequency these variations can be large since the suspended mirror and bench are free to move. To cope with this an additional control loop is added: a rigid reference cavity (RFC) is probed with a pick-off of the beam transmitted by the IMC. The PDH signal in reflection of this cavity is sensitive to laser frequency variations, which are in turn dominated by the IMC length variations, as an effect of the pre-stabilization loop. Therefore the error signal coming from RFC reflection can be used to control mechanically the IMC end mirror, thus stabilizing the low frequency IMC motion to the rigid RFC reference. This has the additional effect of stabilizing the laser frequency to the RFC inside the active band of the mechanical loop. In this way the residual fluctuation of the laser frequency is reduced to few Hz RMS, enough to acquire the interferometer arm lock. The pre-stabilization loop has a band-width of the order of 200 kHz, while the mechanical lock of the IMC on the RFC has a band-width of 100 Hz.

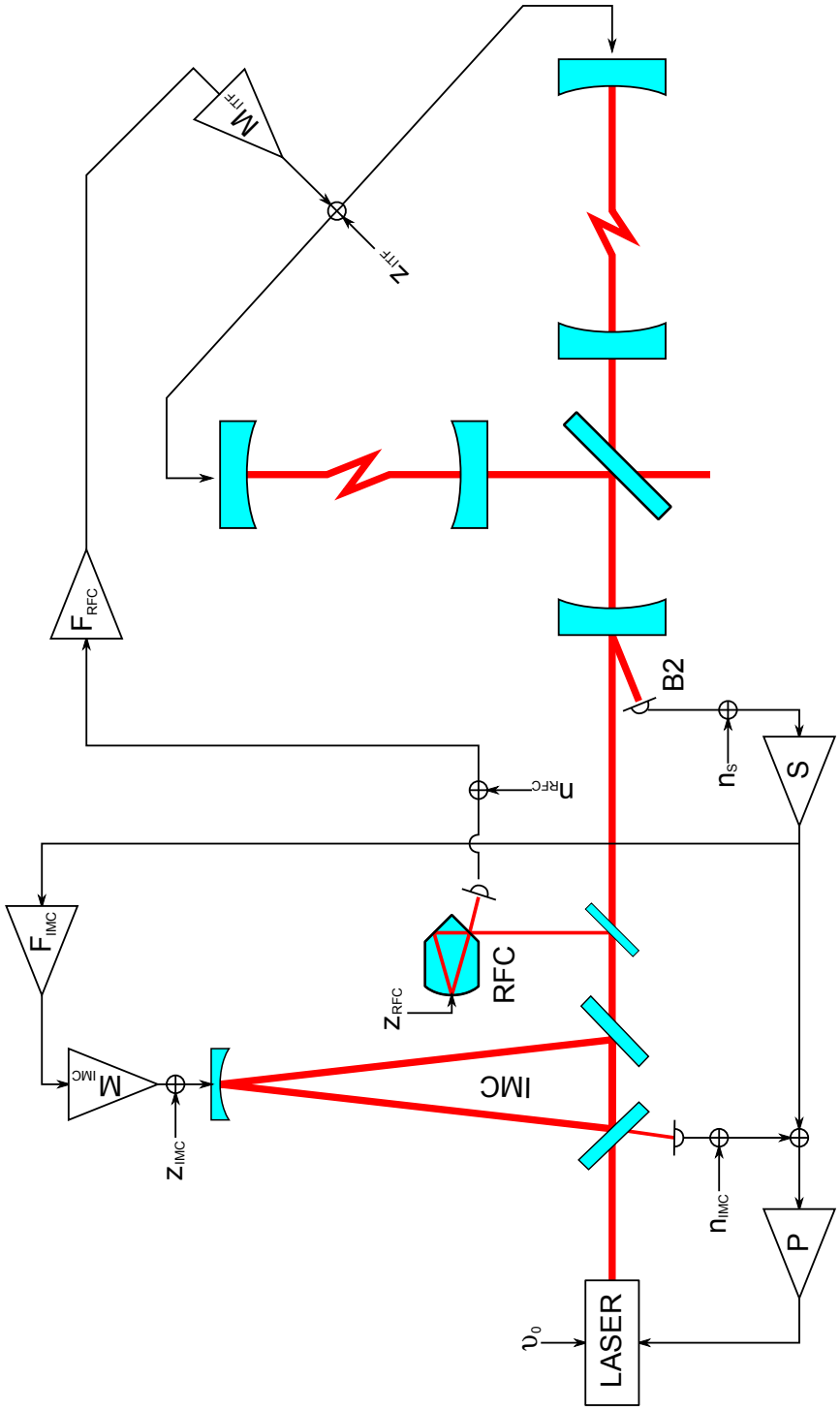

Figure 1: Optical scheme of the second stage of frequency stabilization with the ITF locked.

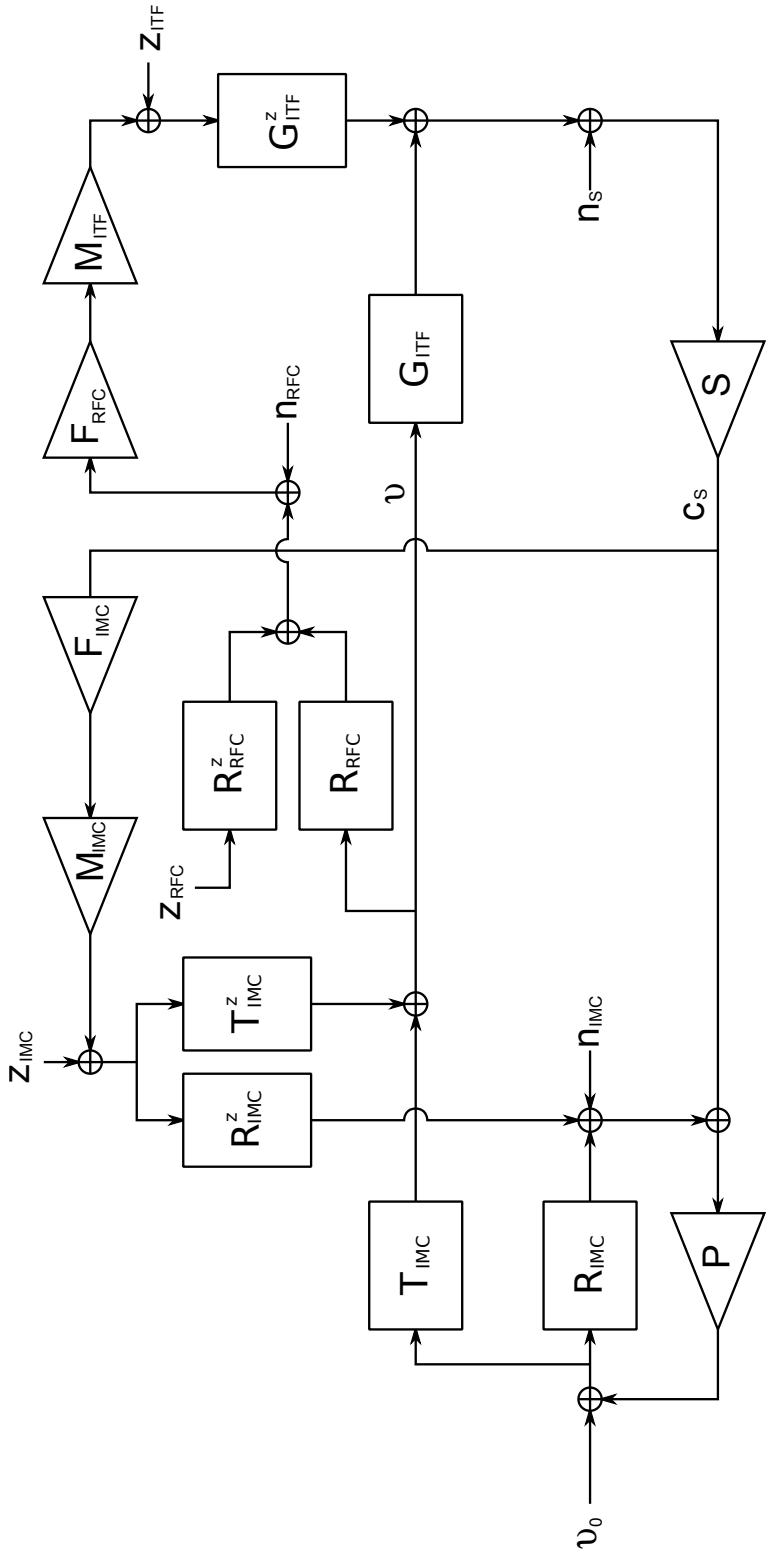

Figure 2: Block diagram of the second stage of frequency stabilization with the ITF locked.

When the full interferometer is locked this stabilization is not enough to meet the requirements. Therefore it is necessary to add an additional stage, which uses as reference the arm itself (fig. 1). This should not be surprising since what is really needed for interferometer purposes is the relative stability between the laser frequency and the arm length. The error signal is extracted in reflection of the power recycling cavity, with different demodulation frequencies depending on the configuration [1]. A controller (S in the figures) is used to compute a correction to be applied to the laser frequency. However, this correction can not be sent to the laser only, otherwise it would move the IMC out of resonance. To cope with this issue an electronic summation point is implemented: the SSFS correction is summed with proper gain with the PDH signal in reflection of the IMC and this is used as error signal for the pre-stabilization loop. In other words, with respect to the stand-alone configuration of the injection system, the SSFS correction is added to the IMC reflection. At those frequencies where the gain of the pre-stabilization loop is much larger than one, its own error signal is squeezed to zero: in other words the effect of the pre-stabilization loop is to force the reflection of the IMC and the SSFS correction signals to be opposite. In this condition the SSFS correction itself resembles the IMC reflection and is therefore sensitive to any longitudinal motion of the IMC cavity out of resonance. The SSFS correction can therefore be used as error signal for the mechanical lock of the IMC, thus substituting the RFC. In this configuration the laser frequency follows the interferometer 3 km long arm cavity inside the SSFS band-width, typically 20-30 kHz, and the IMC length above this frequency and inside the band-width of the pre-stabilization. Moreover the IMC is maintained locked at resonance with respect to the laser frequency with a band-width of about 100 Hz, more than enough to stabilize the low frequency mirror and bench motions.

This configuration would be enough to ensure a proper matching of the laser frequency and the arm length, with residual relative fluctuations dictated only by the SSFS loop performances. However, the low frequency motion of the cavities common mode is left free to move. Even if the mirrors are suspended to the super-attenuators, their low frequency motion can be as large as some fractions of microns, which would result in a slow jitter of the laser frequency by many kHz following the arm cavity length variations. It is desirable to reduce this low frequency jitter of the laser a much as possible, mainly due to the presence of the output mode cleaner, which is an additional cavity at the output of the interferometer which must also be resonant for the laser field with good accuracy. Any fluctuation of the frequency would result in a loss of accuracy of the OMC resonance, which in turn can couple OMC noise into the detector sensitivity [3].

An additional loop is therefore implemented, using the reference cavity reflection signal to control mechanically the arm cavity common mode, with a bandwidth of few Hz. Indeed the RFC reflection is sensitive to laser frequency variations, but these in turn are dominated by arm cavity low frequency motion. An additional reason to have this loop active is the ability of fully reconstruct each cavity length variations that can be used in the global inverted pendulum control system (GIPC).

2.2 Definition of terms

Fig. 2 shows a block diagram of all the optical, mechanical and control transfer functions involved in the full frequency stabilization system:

T_{IMC} optical transfer function of the input mode cleaner: transmission from input frequency noise to output frequency noise [Hz/Hz];

R_{IMC} input mode cleaner transfer function from input frequency noise to reflection port demodulated signal [V/Hz]: the product of the optical response [W/Hz] and the photo-diode response [V/W];

R^z_{IMC} input mode cleaner response of the reflection port demodulated signal to longitudinal motion of the cavity [V/m]: the product of the optical response [W/m] and the photo-diode response [V/W];

T^z_{IMC} transfer function of the input mode cleaner from cavity longitudinal motion to frequency noise in transmission [Hz/m];

P pre-stabilization correction loop, including the laser actuation [Hz/V];

R_{RFC} response of reference cavity reflection demodulated signal to input laser frequency [V/Hz]: the product of the optical response [W/Hz] and the photo-diode response [V/W];

R^z_{RFC} response of reference cavity reflection demodulated signal to cavity length [V/m]: the product of the optical response [W/m] and the photo-diode response [V/W];

M_{IMC} mechanical actuation response of the IMC end mirror, including coil drivers [m/V];

F_{IMC} control filter for the input mode cleaner longitudinal control loop [V/V];

F_{RFC} control filter for the CARM lock to reference cavity signal [V/V];

M_{ITF} mechanical response of the CARM control with end mirrors, including coil drivers [m/V];

G_{ITF} full ITF optical transfer function from input laser frequency to SSFS error signal [V/Hz]: the product of the optical response [W/Hz] and the photo-diode response [V/W];

G^z_{ITF} response of the full ITF to end mirror CARM motion, as seen by SSFS error signal [V/m]: the product of the optical response [W/m] and the photo-diode response [V/W];

S control filter for the second stage of frequency stabilization [V/V];

ν_0 free running laser frequency noise [Hz/$\sqrt{\text{Hz}}$];

ν laser frequency noise at the interferometer input [Hz/$\sqrt{\text{Hz}}$];

n_{IMC} total sensing noise in the input mode cleaner reflection demodulated signal [V/$\sqrt{\text{Hz}}$];

n_{RFC} total sensing noise in the reference cavity reflection demodulated signal [V/$\sqrt{\text{Hz}}$];

n_S total sensing noise in the ITF demodulated SSFS error signal [V/$\sqrt{\text{Hz}}$];

z_{IMC} IMC length noise [m/$\sqrt{\text{Hz}}$];

z_{RFC} RFC length noise [m/$\sqrt{\text{Hz}}$];

z_{ITF} ITF length noise for the CARM degree of freedom [m/$\sqrt{\text{Hz}}$];

2.3 System equations

From the block scheme of fig. 2 one can get the basic equations that links the frequency noise at the interferometer input with all the control loops and input noise sources:

$$\begin{aligned}
\nu &= T^z_{IMC}\left[z_{IMC} + M_{IMC}F_{IMC}c_s\right] + T_{IMC}\nu_P \\
\nu_P &= \nu_0 + P\left[c_s + n_{IMC} + R_{IMC}\nu_P + R^z_{IMC}\left(z_{IMC} + M_{IMC}F_{IMC}c_s\right)\right] \\
c_s &= S(n_s + G^z_{ITF}z_{ITF}) + SG^z_{ITF}M_{ITF}F_{RFC}(n_{RFC} + R^z_{RFC}z_{RFC}) + S(G_{ITF} + G^z_{ITF}M_{ITF}F_{RFC}R_{RFC})\nu
\end{aligned}$$

where in addition to the previous definitions, ν_P is the laser frequency measured before the IMC and c_s is the second stage of frequency stabilization correction. The first equation can be solved for ν_P:

$$\nu_P = \frac{\nu}{T_{IMC}} - \frac{T^z_{IMC}}{T_{IMC}}\left(z_{IMC} + M_{IMC}F_{IMC}c_s\right) \tag{2.1}$$

Substitution into the second equation, together with use of the third equation, yields the final result:

$$\begin{aligned}\nu = \frac{1}{1 - O_P - G_P S\,(G_{ITF} + G_{RFC})} \quad & \Big[\quad T_{IMC}\nu_0 + G_P S\, G^z_{ITF} z_{ITF} \\ & + \quad \left((1 - O_P)\, T^z_{IMC} + \frac{T_{IMC}}{R_{IMC}} O_P R^z_{IMC} \right) z_{IMC} \\ & + \quad \frac{T_{IMC}}{R_{IMC}} O_P n_{IMC} + G_P S n_S \\ & + \quad G_P S \frac{G_{RFC}}{R_{RFC}} \left(n_{RFC} + R^z_{RFC} z_{RFC} \right) \Big]\end{aligned} \tag{2.2}$$

where some new terms have been defined as follows:

$$O_P = P R_{IMC} \tag{2.3}$$
$$O_{IMC} = -R^z_{IMC} M_{IMC} F_{IMC} \tag{2.4}$$
$$C^z_{IMC} = T^z_{IMC} M_{IMC} F_{IMC} \tag{2.5}$$
$$G_{RFC} = G^z_{ITF} M_{ITF} F_{RFC} R_{RFC} \tag{2.6}$$
$$G_P = (1 - O_P)\, C^z_{IMC} + \frac{T_{IMC}}{R_{IMC}} O_P\, (1 - O_{IMC}) \tag{2.7}$$

where O_P is the open-loop transfer function of the pre-stabilization path; O_{IMC} is the open loop transfer function of the IMC mechanical lock; C^z_{IMC} is the coupling of SSFS correction to laser frequency through the IMC mechanical lock; G_{RFC} is the coupling of frequency noise to the interferometer signal through the RFC lock; G_P is the transfer function from SSFS correction to laser frequency through the pre-stabilization loop.

3 Requirements on laser frequency at ITF input

The main figure of merit of the second stage of frequency stabilization is the level of frequency noise at the interferometer input. The tolerable amount of frequency noise is computed from Optickle simulations [6] of the coupling of frequency noise to the dark fringe signal. A limit of a factor 10 below the target detector sensitivity is used to compute the requirement on frequency noise. The coupling of frequency noise to dark fringe depends on the interferometer configuration (power recycled or dual recycled) and on interferometer defects (like losses and finesse asymmetries). Figure 3 shows the resulting upper limits in input of the interferometer, computed as the minimum over few cases of interferometer asymmetries (losses asymmetry up to 50 ppm and finesse asymmetry up to 2%).

4 Input ingredients

4.1 Optical transfer functions

To compute requirements and performances the optical responses already described in the previous section 2.2 are needed. They are obtained from simulations done with Finesse [4] for the IMC and RFC and with Optickle [5] for the interferometer transfer functions, since radiation pressure effects are in that case relevant.

The interferometer response to frequency noise at its input is shown in fig. 4 in the case of power recycled interferometer at 25 W and dual recycled interferometer at 125 W. In the power recycling case, as expected, the transfer function shows structures around few tens of kHz that must be compensated in the control loop to be able to push the unity gain frequency up to 20-25 kHz. Surprisingly, the dual recycled case does not show any shape in the transfer function, which simply drops as 1/f. The only common feature is the notch at the free

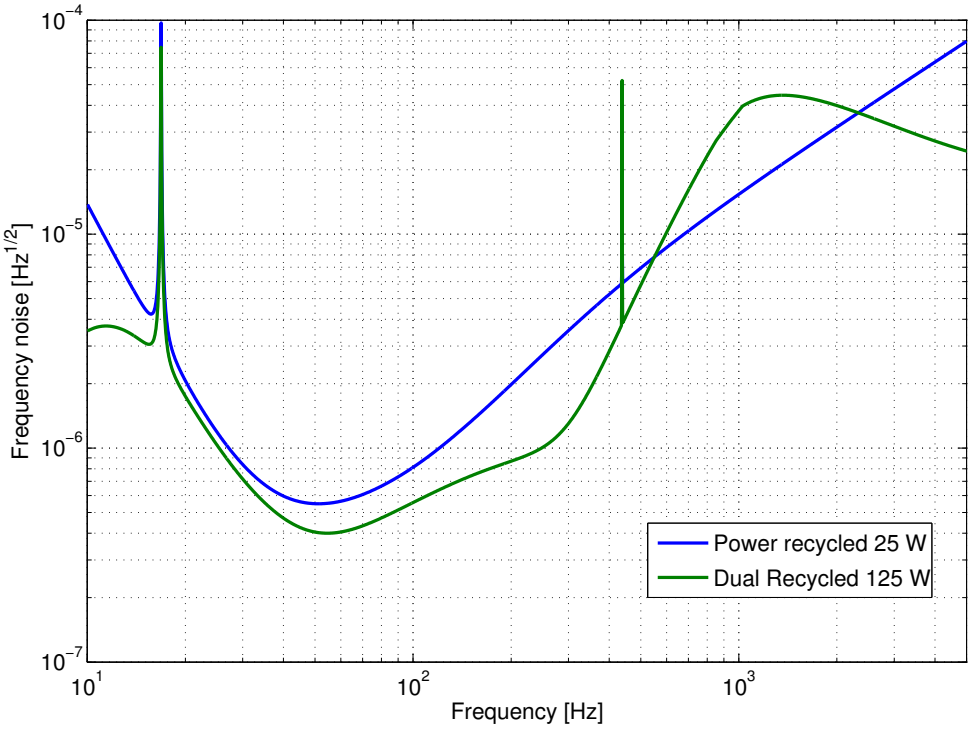

Figure 3: Requirements for frequency noise at the interferometer input, in two possible working configurations.

spectral range, which is at about 50 kHz in the Advanced Virgo case. This is the final limit on the gain of the frequency stabilization loop. In the dual recycled case, the low frequency region is modified due to radiation pressure effects.

4.2 Actuation transfer functions

There are three actuation points involved in the frequency stabilization loop. The faster one is the laser frequency actuation, which is in the Virgo master laser had a gain of about 1.5 MHz/V [7]. The other two points are mechanical and acts on the IMC end mirror and on the interferometer terminal mirrors. In both case a pendulum response is assumed with resonant frequency at 0.6 Hz and DC actuation gain of 15 μm/V. In reality the interferometer CARM actuation response will be more complex, since a fraction of the force will be re-allocated to the marionette. However, this is neglected here since it simply adds complexity to the design of the slow CARM control loop, but it poses no conceptual difficulties.

5 Control filters and stability

The laser frequency pre-stabilization loop will have a band-width of the order of 200 kHz, the gain will go like 1/f between 200kHz to 30kHz, and like $1/f^4$ below 30kHz [7]. The parameters of the corresponding control filter are shown in tab. 1.

The input mode cleaner mechanical lock had a band-width of about 100 Hz in Virgo+. The same bandwidth is assumed for Advanced Virgo. The corresponding control filter is detailed in tab. 1.

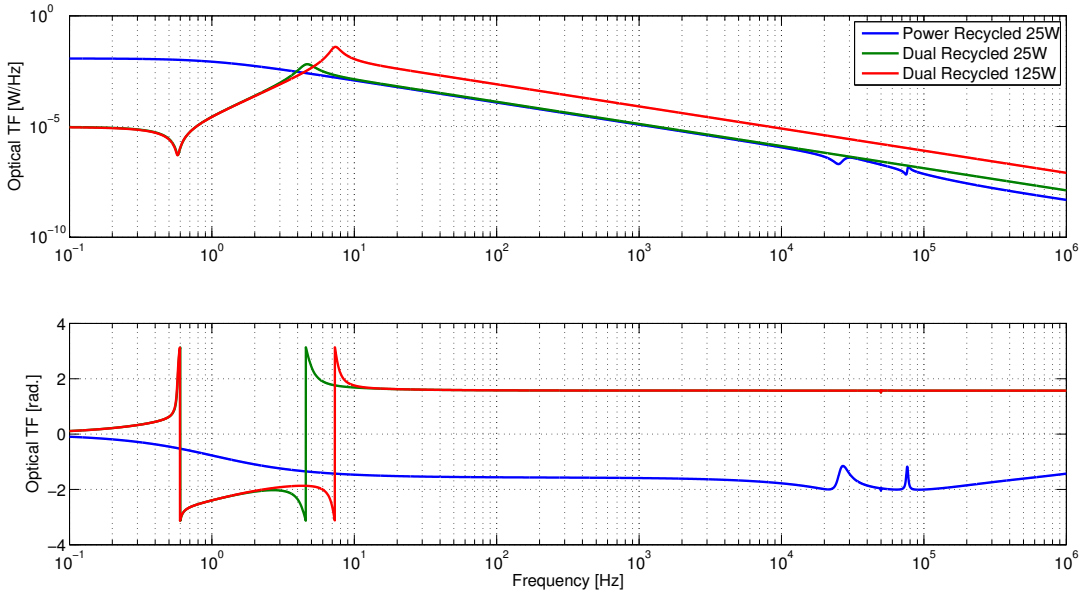

Figure 4: Transfer function from frequency noise at ITF input to frequency stabilization error signal.

Finally the CARM lock on the reference cavity will have, like in Virgo+, a band-width of few Hz. As before the control filter parameters are listed in tab. 1.

The gains of all the controllers have been adjusted to obtain correct stable open loop transfer functions. In the case of the pre-stabilization loop and the IMC mechanical lock these OLTF are given by equations 2.3 and 2.4. In the RFC case the open loop transfer function is given by:

$$O_{RFC} = R_{RFC} F_{RFC} M_{ITF} \frac{G^z_{ITF}}{G_{ITF}} \tag{5.1}$$

where the last term is introduced to model the fact that at low frequency, where the RFC loop is relevant, the mechanical motion of CARM is directly converted to frequency noise at the interferometer input (which is the same at RFC input) by the high gain of the SSFS loop. This ratio is equal, at least at frequencies much lower than the free spectral range, to the ratio between laser frequency and cavity length:

$$\frac{G^z_{ITF}}{G_{ITF}} \sim \frac{\nu_{LASER}}{L} \sim 10^{11}\text{Hz/m} \tag{5.2}$$

The stability of SSFS loop can be analyzed considering its nested configuration. The properties of a nested loop are reported in fig. 5, where it is shown how it can be decomposed in the product of two loops. The complete scheme of SSFS loop is quite complex, as it is inferred from figures 1 and 2. It is useful to reduce it to recover the main components of the nested loops, which will be important to asses the global stability of the system. The reduction procedure is presented in figures 6 and 7, using the transfer functions defined in equations from 2.3 to 2.7. The reduction shows that the nested loop is composed by the multiplication of the closed loop of the pre-stabilization stage $\frac{1}{1-O_P}$ and the transmission of the IMC cavity T_{IMC}, closed with the nesting function O_S :

$$O_S = \left[\frac{O_P}{R_{IMC}} \cdot (1 - O_{IMC}) + C^z_{IMC} \frac{(1 - O_P)}{T_{IMC}} \right] \cdot S \cdot [G_{ITF} + G_{RFC}] \tag{5.3}$$

The nesting function is proportional to the correction filter S, to the sum of the implied interferometer's transfer functions G_{ITF} and G_{RFC}, and the sum of the two correction paths: the first, with transfer function

$$W1 = O_P R_{IMC}(1 - O_{IMC}) \tag{5.4}$$

really nesting on the pre-stabilization loop (directly on the laser or by changing the set point via the IMC) and the second

$$W2 = C^z_{IMC} * \frac{(1 - O_P)}{T_{IMC}} \tag{5.5}$$

closing at the IMC and taking into account the correction on the frequency due to IMC length variation (i.e. C^z_{IMC}). Using the transfer function G_P defined previously, the nesting function O_S can also be written as:

$$O_S = \frac{G_P}{T_{IMC}} * S * [G_{ITF} + G_{RFC}] \tag{5.6}$$

The global closed loop transfer function:

$$CLTF = \frac{T_{IMC}}{1 - O_P} \frac{1}{1 - \frac{T_{IMC}}{1-O_P}\left[\frac{O_P}{R_{IMC}}(1 - O_{IMC}) + C^z_{IMC}\frac{(1-O_P)}{T_{IMC}}\right] S\,[G_{ITF} + G_{RFC}]} \tag{5.7}$$

can thus be considered as the product of the two loops: the first related to O_P and the second to the nesting effective function

$$O_N = \frac{T_{IMC}}{1 - O_P}\left[\frac{O_P}{R_{IMC}}(1 - O_{IMC}) + C^z_{IMC}\frac{(1 - O_P)}{T_{IMC}}\right] S\,[G_{ITF} + G_{RFC}] \tag{5.8}$$

The effective nesting function O_N can be rewritten also as

$$O_N = G_P S\,(G_{ITF} + G_{RFC})\,\frac{1}{1 - O_P} \tag{5.9}$$

which makes in evidence the role of G_P, already defined as the transfer function from SSFS correction to laser frequency through the pre-stabilization loop.

The effective loops O_P and O_N are engaged in series; this is the reason why the stability is requested to both and not only to the nested configuration, whose open loop O_G, that can be obtained also by performing the multiplication in CTLF and expliciting, is given by $O_G = O_P + G_P . * S . * (G_{ITF} + G_{RFC})$, as also shown in eq. 2.2.

The first loop to be considered is the pre-stabilization loop, called O_P. It is engaged before the SSFS and it is maintained after the engagement of the SSFS. The open loop transfer function is reported in fig. 8. The unity gain is at 250 kHz.

The second loop is O_N which is the SSFS loop as it enters in the nested configuration. Its transfer function is reported in fig. 9. The unity gain is at 20 KHz, the phase margin is than 53 degrees.

The transfer function of the global loop O_G, is reported in fig. 10. It can be seen that the unity gain is defined by the fast loop while the lower frequency gain in greatly enhanced by the SSFS.

6 Sensing and ADC-DAC noises

The sensing noise of each photo-diode signal is assumed to be at the shot noise level, given the following powers impinging on the diodes: 100 mW on the IMC reflection, 25 mW on the RFC reflection and 100 mW on the SSFS error signal diode (B2, interferometer reflection). In this first version of the note the photo-diode responses

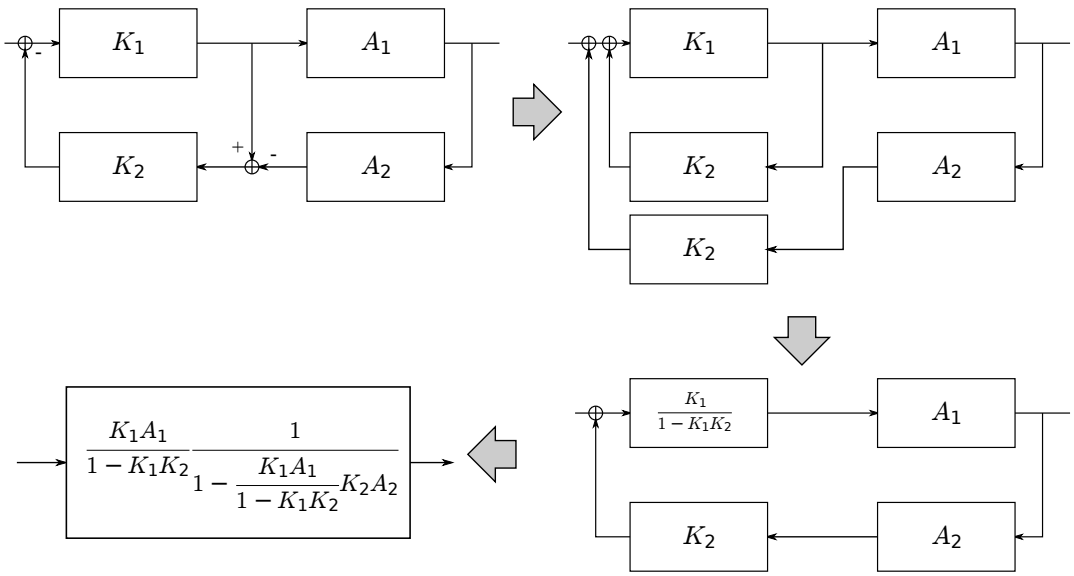

Figure 5: Scheme of a nested loop and example of the steps needed to reduce it to a normal, single branch, loop.

(V/W) is not considered and all sensing noises are expressed in units of W. In the future the conversion factors will be considered to estimate the needed dynamical range of all signals involved in the laser stabilization.

An estimate of the input mode cleaner length noise has been obtained from Virgo+ data [8] and it is shown in fig. 11.

The laser frequency noise in free running configuration is modeled to be of the order of [2]:

$$\nu_0 = 100 \cdot \left(\frac{100\ \text{Hz}}{f}\right)\ \text{Hz/Hz}^{-1/2} \tag{6.1}$$

Considering the remarkable dynamic of the loops, other important contributions that must be evaluated are the noise floors of ADCs and DACs. These noises have been taken into account assuming for the ADC a sampling frequency of 0.5 MHz and 15 (real) bits and covering, in closed loop, 1/10 of the ADC dynamic with the simulated RMS signal. The ADC noise is considered to be the quantization noise, calculated with the usual formula:

$$V_n = \frac{q}{\sqrt{12}}\frac{1}{\sqrt{f_s/2}}\text{V}/\sqrt{\text{Hz}} \tag{6.2}$$

.

Inserting the noise in the loop, under these assumptions the quantization noise turns out to be negligible, as it is shown in fig. 13. Similar considerations have been applied to the DAC noise, at the output of SSFS board. It has been considered again that the DAC range will be covered no more than 1/10 by the signal. The expected noise has been calculated as $300nV/\sqrt{Hz}$ for a DAC with 10 V of dynamic range. Before considering the noise projections it is interesting to note the contributions to the correction signal at the SSFS output. These are shown in fig. 12. The main contribution at the SSFS output in low and intermediate frequencies derives from the correction of the IMC lenght noise. This is expected, because the first stage of stabilization, the pre-stabilization, locks the laser frequency on the IMC lenght. At higher frequencies the correction is dominated by the SSFS error signal and by the residual free-laser frequency noise, which is not suppressed by the pre-stabilization stage

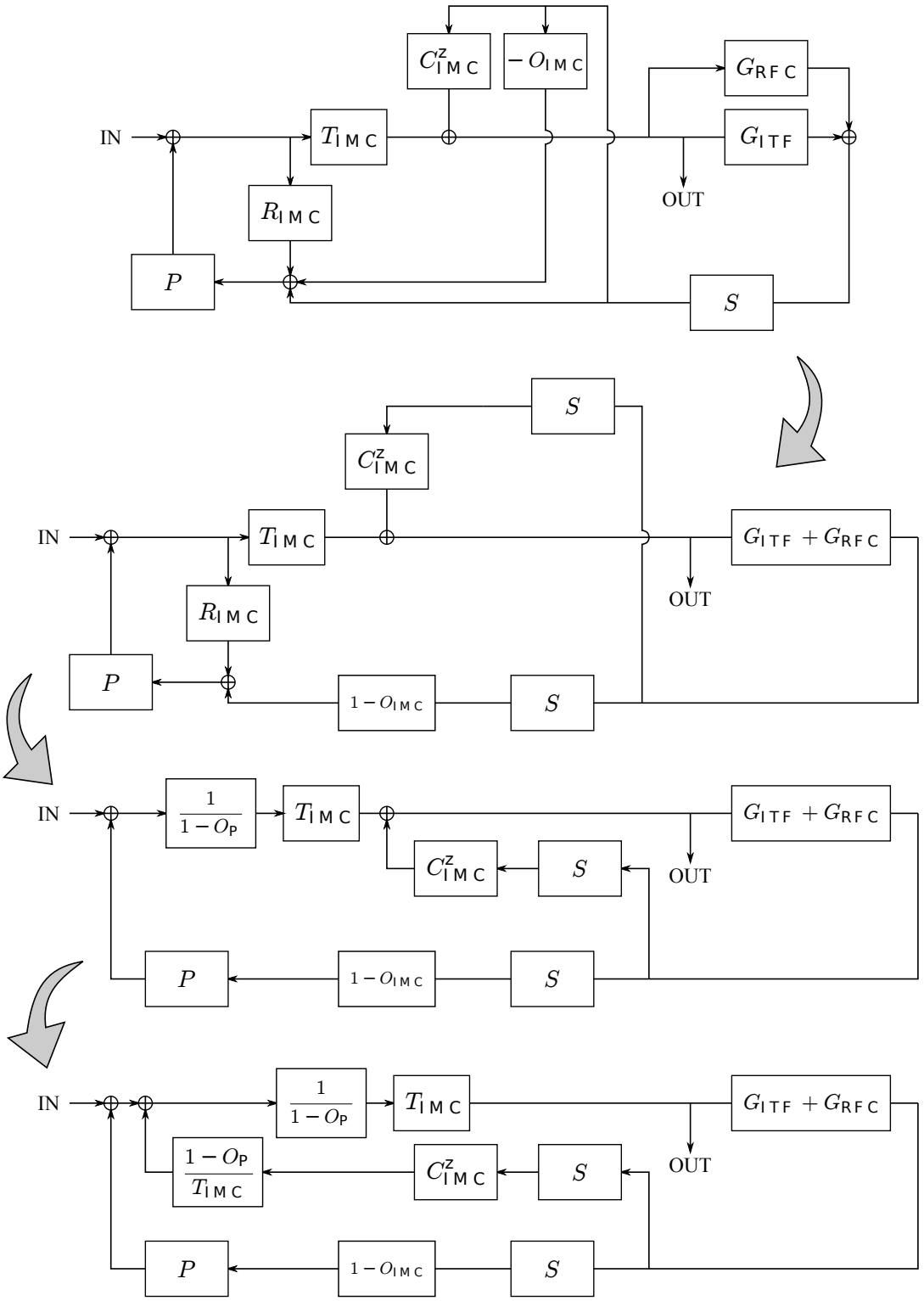

Figure 6: First part of the steps needed to reduce all the nested frequency stabilization loops to a standard, one branch, loop. Continues in fig. 7

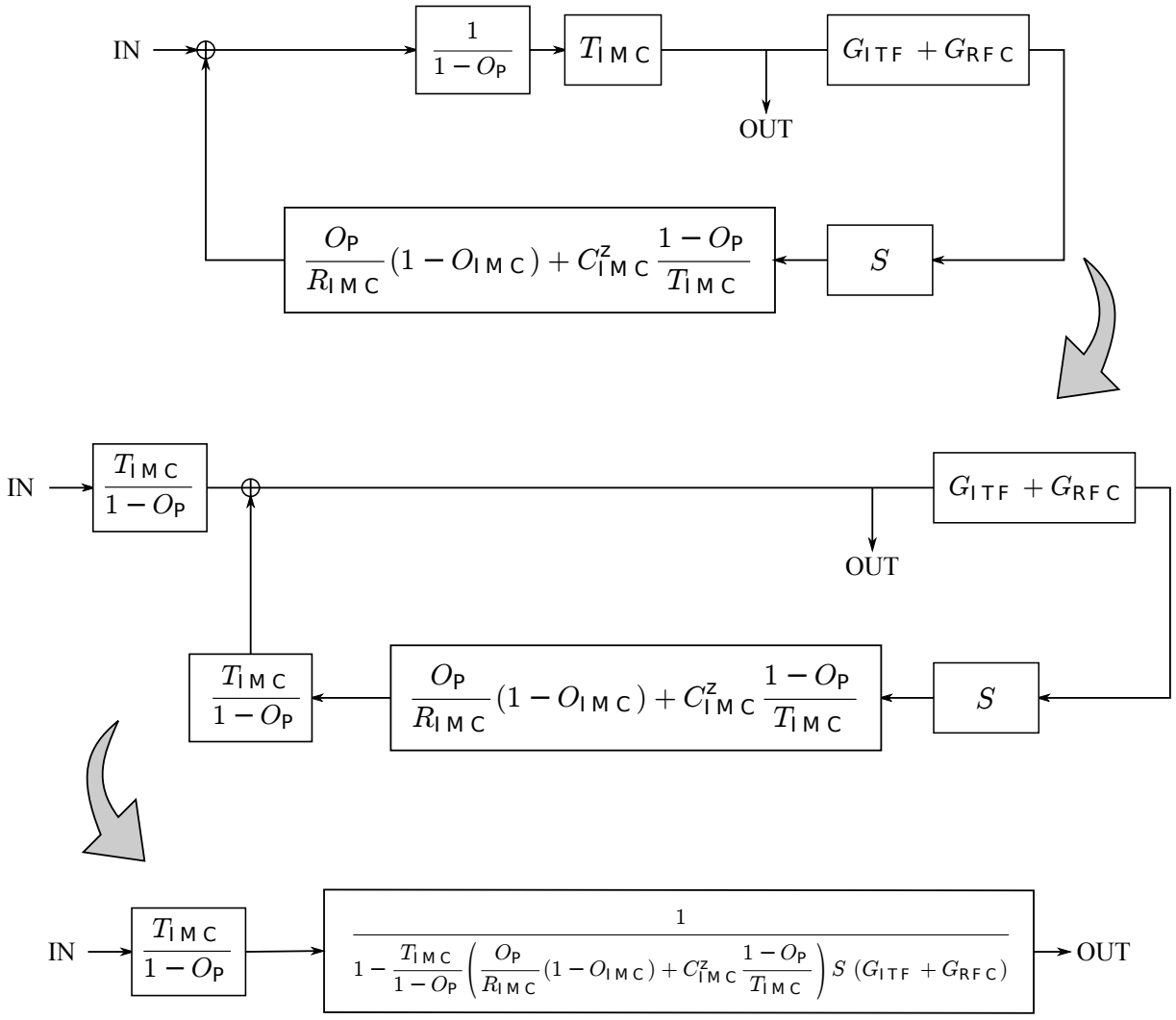

Figure 7: Second part of the steps needed to reduce all the nested frequency stabilization loops to a standard, one branch, loop. Continues from fig. 6

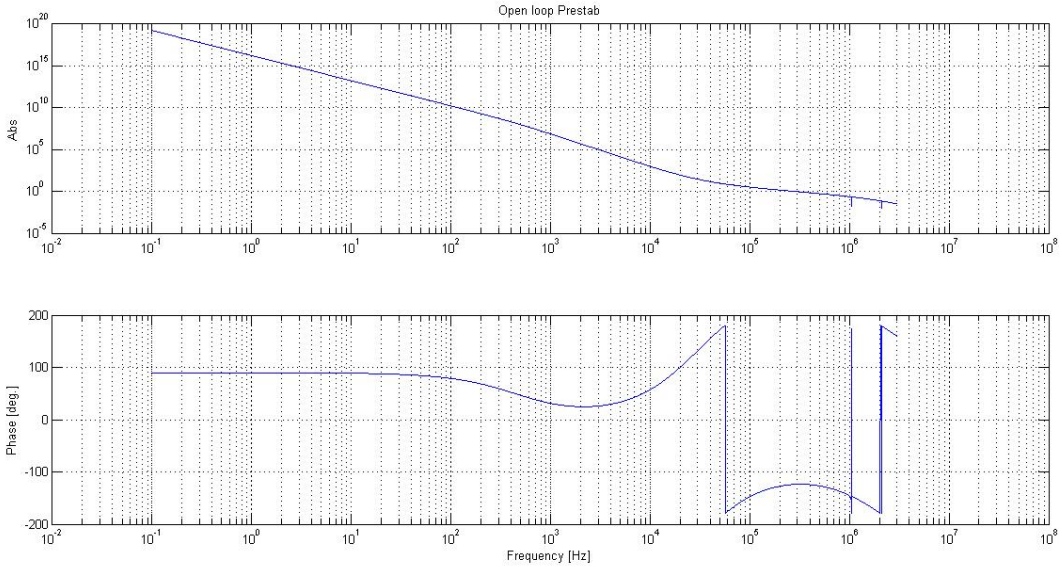

Figure 8: Open loop transfer function of the pre-stabilization stage

because of the lower gain of the loop. Finally it can be noticed that the correction coming from the ADC noise is negligible, because in these assumptions the ADC noise is a couple of order of magnitudes lower than B5 shot noise error signal and also the DAC noise correction is negligible.

7 Noise projections

Using equation 2.2 it is possible to compute the contribution of each noise source to the frequency noise at the interferometer input. The total has to be compared to the requirements of fig. 3. Two cases has been studied: dual recycled at 125 W and power recycled only at 25 W.

Results in the dual recycled case are shown in fig. 13. As expected the largest contribution comes from the shot noise of the SSFS error signal, which is B2 in this configuration. This contribution is nevertheless compliant with

Degree of freedom	Gain	Zero freq. [Hz]	Zero Q	Pole freq. [Hz]	Pole Q
IMC	0.23 V/V@ 100 Hz	15	0	0	0
		30	1	0	0
				300	0.7
Pre-stabilization	$73 \cdot 10^3$ Hz/V @ 200kHz	$22 \cdot 10^3$	0	0	0
		$37 \cdot 10^3$	0.5	0	0
				0	0
				$2.2 \cdot 10^6$	0.5
RFC	-0.92 V/V @ 1 Hz	0.25	0.5	0	0
		0.6	0	0	0
				8	0.5
SSFS	$-5.56 \cdot 10^3$ V/V @ 10 kHz	$3.62 \cdot 10^3$	0.5	0	0
				$9.55 \cdot 10^4$	0.5

Table 1: Control filters for the pre-stabilization, IMC and RFC loops.

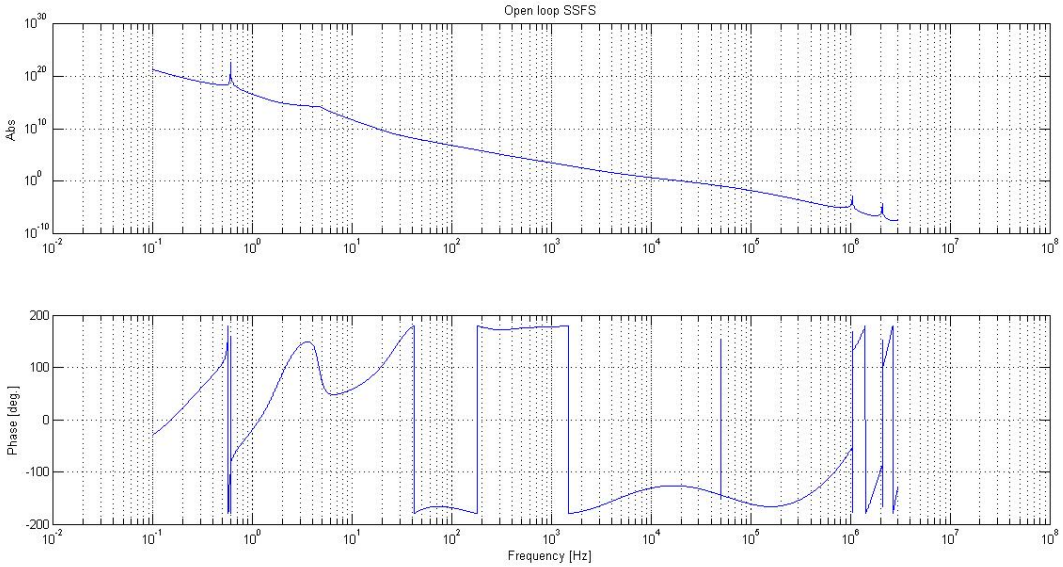

Figure 9: Open loop transfer function of the SSFS stage

the requirements. The frequency noise requirements depend on the coupling of frequency noise to the detector sensitivity. This in turn depends on the interferometer asymmetries. Here only losses and finesse asymmetries have been considered. The coupling increases when introducing asymmetries [6], but the effect is not as large as to limit the detector sensitivity.

Results in the power recycled case are shown in fig. 14. As before the largest contribution comes from the shot noise of the SSFS error signal, which is again B2. Fig. 14 shows several requirement curves, corresponding to different asymmetries. Assuming, as in the dual recycled case, losses asymmetries of 50 ppm and finesse asymmetry of 2% gives requirements which can't be fulfilled by the frequency stabilization system. In particular in the intermediate frequency region the SSFS error signal shot noise is about a factor 2 above the requirements. To recover this factor on the SSFS side it would be necessary to increase the total power impinging on the SSFS error signal diodes to 400 mW, which seems not feasible.

On the other hands, assuming the SSFS error signal to be limited by the shot noise corresponding to 100 mW, limits can be put on the maximum possible asymmetries. They are 40 ppm of losses asymmetries and 1% of finesse asymmetry. The implementation of a technique to tune the cavity finesse (using the input mirror etalon effect) becomes mandatory.

8 Conclusions and next steps

A full model of the frequency stabilization system in Advanced Virgo has been developed, based on system equations and on simulations of the optical response of both the injection system and the interferometer.

Assuming the SSFS error signal (B2 demodulated at 6 or 8 MHz) to be dominated by the shot noise corresponding to 100 mW total power impinging on the photo-diodes (and thus assuming electronic noise, including SSFS board, to be negligible), the stabilization system is compliant with the requirements in the dual recycled case, without significant limits on interferometer asymmetries.

In the power recycled case instead, to be compliant with the requirements it is necessary to pose limits on the interferometer asymmetries: less than 40 ppm losses asymmetry and less than 1% finesse asymmetry. The latter

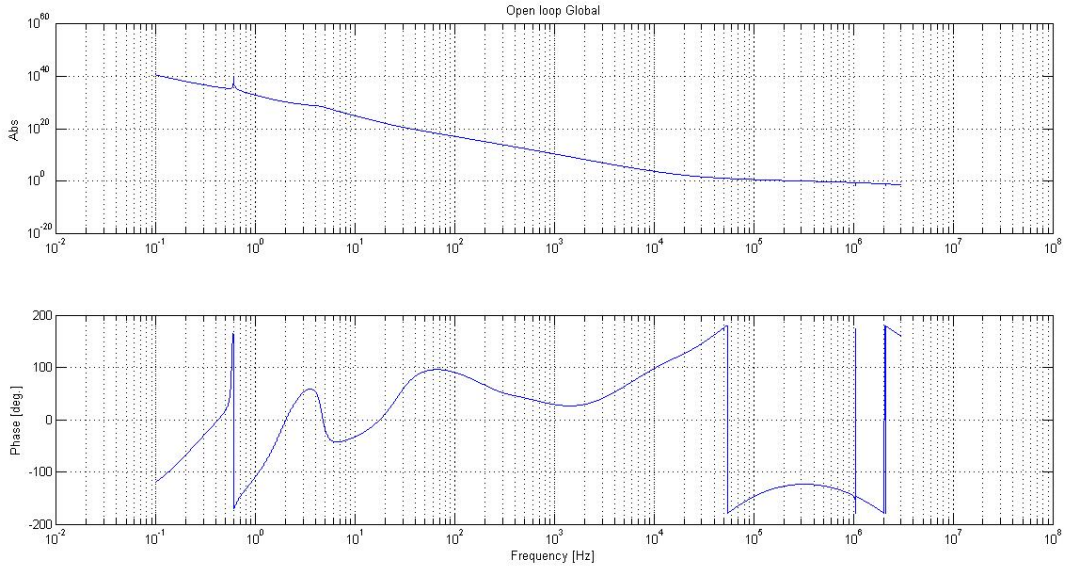

Figure 10: Open loop transfer function of the global SSFS stabilization

requirement makes mandatory the implementation of an active system to control the cavity finesses, using the input mirror etalon effect.

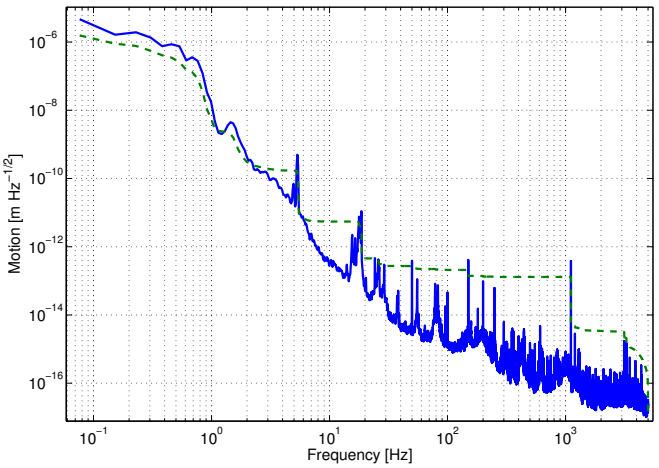

Figure 11: Estimation of input mode cleaner length noise. Dashed line is the integrated RMS.

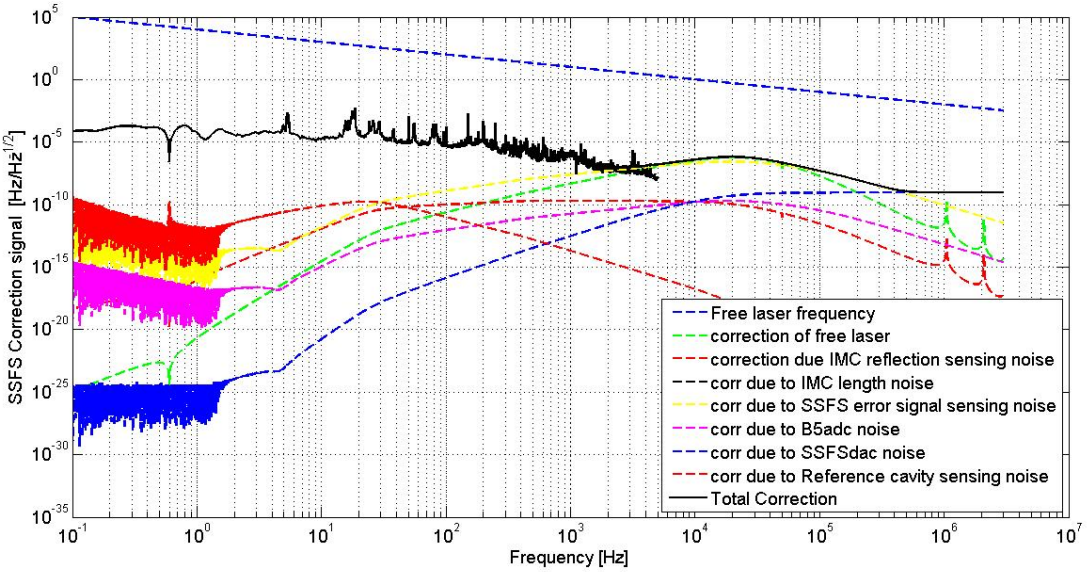

Figure 12: Correction signal at the SSFS output

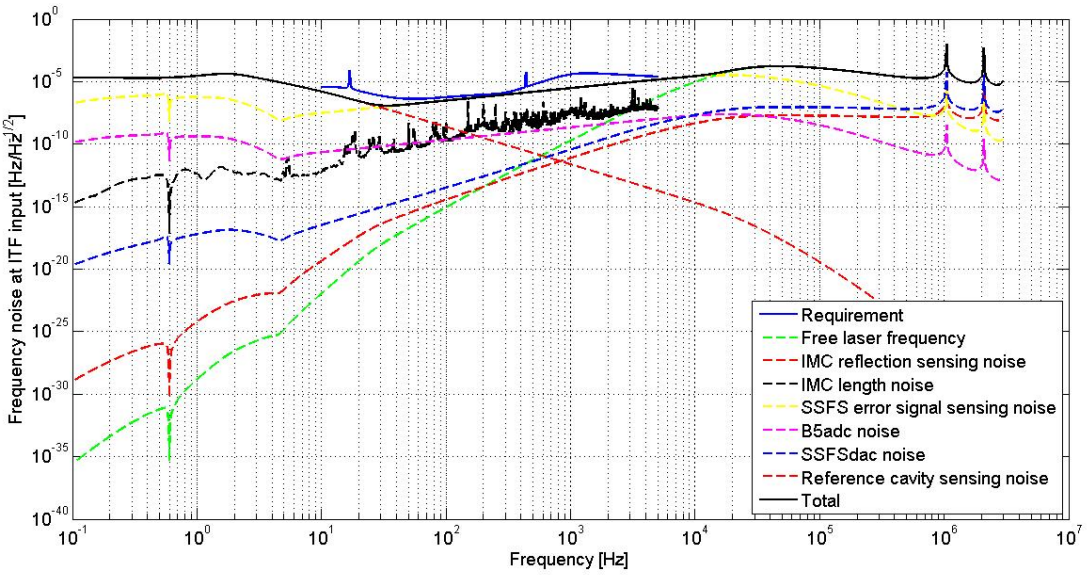

Figure 13: Projection of SSFS noise to residual frequency noise at the interferometer input, compared with requirements, in dual recycled case at 125 W of input power.

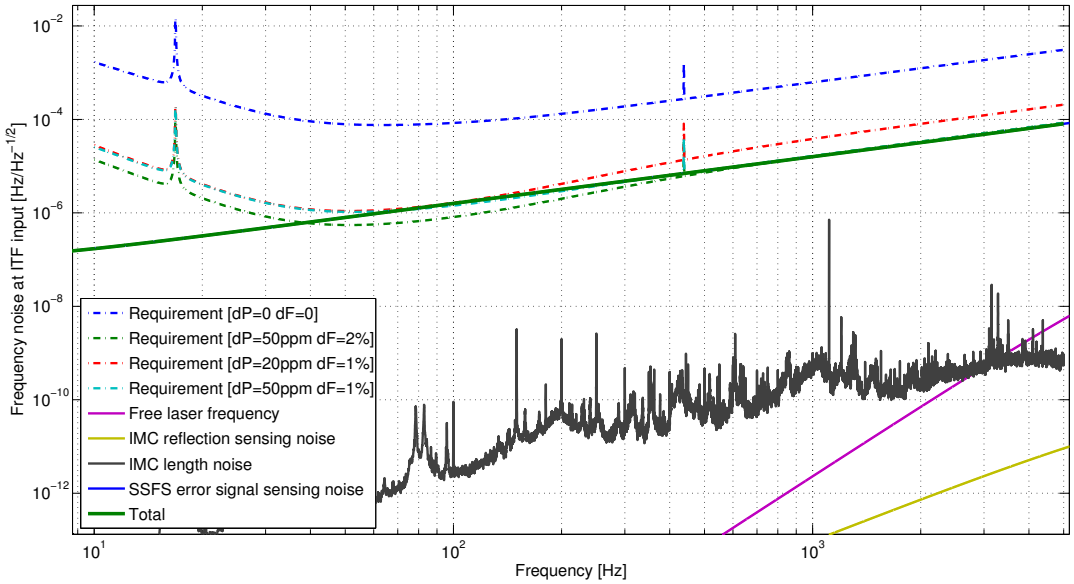

Figure 14: Projection of SSFS noise to residual frequency noise at the interferometer input, compared with requirements in some asymmetry configurations, in power recycled case at 25 W of input power.

References

[1] G. Vajente, *Advanced Virgo Length Sensing and Control steady state design*, VIR-0738A-11 (2011) 1, 4

[2] F. Bondu, *L'interferometre Virgo: proprietes optiques, stabilisation en frequence du laser*, Memoire d'habilitation a diriger des recherches, Observatoire de la Cote d'Azur (2008) 1, 10

[3] E. Tournefier, *Advanced Virgo output mode cleaner: specifications*, VIR-0071A-08 (2008) 4

[4] A. Freise, at al. , *Frequency domain interferometer simulation with higher-order spatial modes*, Class. Quant. Grav. 21 (2004) S1067 [arXiv:gr-qc/0309012] 6

[5] Optickle home-page, http://ilog.ligo-wa.caltech.edu:7285/advligo/ISC_Modeling_Software 6

[6] A. Chiummo, *Coupling of frequency and power noise vs. ITF asymmetries: preliminary results*, VIR-0485A-11 6, 14

[7] F. Cleva, personal communication 7

[8] P. Ruggi, personal communication 10